AD_____

Award Number: DAMD17-01-1-0216


TITLE: Ultrasound Assisted Optical Imaging


PRINCIPAL INVESTIGATOR: Nan Guang Chen, Ph.D.
                        Quing Zhu, Ph.D.


CONTRACTING ORGANIZATION: The University of Connecticut
                          Storrs, Connecticut 06269-4133


REPORT DATE: May 2003


TYPE OF REPORT: Annual Summary


PREPARED FOR: U.S. Army Medical Research and Materiel Command
              Fort Detrick, Maryland 21702-5012


DISTRIBUTION STATEMENT: Approved for Public Release;
                        Distribution Unlimited


The views, opinions and/or findings contained in this report are
those of the author(s) and should not be construed as an official
Department of the Army position, policy or decision unless so
designated by other documentation.

20030902 136

# REPORT DOCUMENTATION PAGE

| 1. AGENCY USE ONLY (Leave blank) | 2. REPORT DATE<br>May 2003 | 3. REPORT TYPE AND DATES COVERED<br>Annual Summary (1 May 2002 – 30 Apr 2003) |
|---|---|---|

**4. TITLE AND SUBTITLE**
Ultrasound Assisted Optical Imaging

**5. FUNDING NUMBERS**
DAMD17-01-1-0216

**6. AUTHOR(S)**
Nan Guang Chen, Ph.D.
Quing Zhu, Ph.D.

**7. PERFORMING ORGANIZATION NAME(S) AND ADDRESS(ES)**
The University of Connecticut
Storrs, Connecticut 06269-4133

E-Mail: chenng@engr.uconn.edu

**8. PERFORMING ORGANIZATION REPORT NUMBER**

**9. SPONSORING / MONITORING AGENCY NAME(S) AND ADDRESS(ES)**
U.S. Army Medical Research and Materiel Command
Fort Detrick, Maryland 21702-5012

**10. SPONSORING / MONITORING AGENCY REPORT NUMBER**

**11. SUPPLEMENTARY NOTES**

**12a. DISTRIBUTION / AVAILABILITY STATEMENT**
Approved for Public Release; Distribution Unlimited

**12b. DISTRIBUTION CODE**

**13. ABSTRACT (Maximum 200 Words)**

Two new diffusive optical imaging systems have been built for improved portability and shorter data acquisition time. We are conducting clinical studies simultaneously at University of Connecticut Health Center and Hartford Hospital with our optical imagers combined with commercial ultrasound. More than 60 patients have been recruited and image initial analysis has been made. Preliminary results have demonstrated the great potential of ultrasound assisted optical imaging in distinguishing malignant tumors from benign lesions. Image reconstruction algorithms based on finite element method have been investigated for better image quality. Novel pseudo-random bit sequence based spread spectrum system architecture is proposed for time-resolved diffusive optical tomography. We have validated the feasibility of such an approach by simulations and experiments. We are planning to use this new technology in our future system upgrade and modification, aiming at more accurate reconstructed values for optical properties of human breast tissues and higher spatial resolution.

**14. SUBJECT TERMS**
Breast cancer, diffusive, ultrasound, near-infrared

**15. NUMBER OF PAGES**
14

**16. PRICE CODE**

| 17. SECURITY CLASSIFICATION OF REPORT<br>Unclassified | 18. SECURITY CLASSIFICATION OF THIS PAGE<br>Unclassified | 19. SECURITY CLASSIFICATION OF ABSTRACT<br>Unclassified | 20. LIMITATION OF ABSTRACT<br>Unlimited |
|---|---|---|---|

# Table of Contents

# Annual Report

PI: Nan Guang Chen

**INTRODUCTION:**

Accurate and efficient detection techniques are crucial for reducing the mortality rate of breast cancer. Currently, X-ray mammography and ultrasound are the most common imaging modalities for breast cancer screening and diagnosis. However, It's hard to differentiate tumors from other lesions such as cysts on an X-ray mammogram. Ultrasound can detect and resolve breast lesions a few millimeters in size, and can distinguish cysts from solid lesions. But the overlapping acoustic characteristics of benign and malignant tumors result in a low specificity of ultrasound. Currently, only 20% patients sent to biopsy have malignant tumors, and 80% patients suffer from unnecessary biopsy. Early detection cannot readily be achieved with current technology. In fact, in most cases it is the patient who first finds the lesion by palpation. Of course, a palpable tumor is generally more than 3 cm in diameter and is no longer at the early stage.

Diffusive optical imaging has been emerging as a potential clinical diagnostic modality. In the last decade, massive research efforts have been made to apply this novel technology to breast cancer detection. The advantages of photon migration imaging include its non-invasive nature, relatively low system costs, and, more importantly, the special specificities it can provide. The optical properties of human tissues in the near infrared region, such as the scattering coefficient and the absorption coefficient, are wavelength dependent and related to the type of tissues, pathological states, and metabolic states. As for the breast cancer detection, the blood volume and blood oxygenation status inside a human breast are associated with different absorption coefficients of oxy-hemoglobin and deoxy-hemoglobin at different wavelengths (such as 780 nm and 830 nm). These optically available parameters can be used to differentiate benign lesions from malignant tumors. However, optical tomography alone suffers from low spatial resolution and target localization uncertainty due to the intensive light scattering inside the tissue. In our current clinical studies, we are combining diffused light imaging with conventional ultrasound in a novel way for detection and diagnosis of solid lesions.

**BODY:**

To facilitate our clinical studies at two sites (University of Connecticut Health Center and Hartford Hospital), we have developed two new near infrared optical tomography systems[1] featuring fast optical switching, three-wavelength excitations, and high dynamic range avalanche photodiode (APD) detectors. Pigtailed laser diodes at 660, 780, and 830 nm are used as light sources and are amplitude modulated at 140 MHz. One 4X1 and one 1X9 optical switches are combined to form a 4X9 switch, which distribute the output of one wavelength to one of nine source fibers. The short switching time (about 3 ms) keeps the data acquisition time within 1 second for a complete scan. This makes it

4

possible to perform near real time imaging and to monitor dynamic physiological changes. The crosstalk between channels is around 60 dB, equivalent to 120 dB in opto-electrical signals. Eight Silicon APD's detect diffusive photon density waves simultaneously. Since the active area of each APD has a diameter of 1.5 mm, an aspherical lens is used to couple the diffusive light collected by a 3 mm diameter light guide to an APD. The dynamic range of APD's is several orders higher than that of PMT's, which is essential for imager using reflection geometry. Since the internal gain of the APD's we are using is 3 orders less than an ordinary PMT, efforts have been made to suppress the feed through interferences from the transmission part to the receiving part so as to reduce the errors in amplitude and phase measurements.

To test the performance of our new imagers, we conducted experiments with various targets. The Intralipid solution mentioned before was used as background media, while spherical targets were located 1.5-3 cm underneath the optical probe. Optical images were obtained with a 1 cm diameter ball positioned 2 cm under the center of the probe and 2 cm in depth. The reduced scattering coefficient of the ball is 9.6 $cm^{-1}$, resulting a diffusion coefficient of 0.0347 $cm^{-1}$. The absorption coefficient of the ball is about 0.2 $cm^{-1}$. The reconstructed images indicate the right location, distribution, and values of both absorption and diffusion heterogeneities. It takes less than 1 second to finish a complete scan for one wavelength. We have moved one of these new imagers to UConn Health Center and keep another in our lab for phantom studies and algorithm development.

We have recruited more than 60 patients in our clinical studies. Initial clinical results by the use of optical tomography assisted with conventional ultrasound demonstrate that there is a huge optical contrast between early stage invasive cancers and benign solid lesions due to angiogenesis[2,3]. An average of 52.6 $\mu$mole difference was obtained between two small invasive cancers and a group of 17 benign solid lesions. In addition, the small invasive cancers were localized well in absorption maps and have shown wavelength-dependent absorption changes while the benign lesions appeared more diffused in absorption maps have shown relatively wavelength-independent absorption changes.

Time-resolved photon migration imaging (TPMI) has the potential to provide higher resolution images and more accurate reconstruction of optical property maps inside human tissues than frequency-domain and continuous-wave optical imaging systems. However, current implementation of TPMI suffers from too long data acquisition time, low signal to noise ratio, and high cost. Consequently, TPMI has not been well studied and its advantages have not been fully demonstrated. We propose a novel system architecture that is totally different from conventional short pulse based systems. It is well known in the communication industry that a pseudo-random bit sequence (PRBS) has a broadband spectrum, and its auto correlation function is similar to that of a short pulse. Recently, code division multiple access (CDMA) is preferred to time division multiple access (TDMA) in wireless communication because of its superior signal to noise ratio, interference rejection, and multiple path rejection. The relation between a pulse based TPMI system and a PRBS based one is analogous to that between CDMA

and TDMA. By using a light source modulated with PRBS's, the temporal point spread function (TPSF) of the subject under investigation can be retrieved with a high signal to noise ratio in a short scan time. In addition, we expect that the system cost will be significantly reduced.

Time-resolved measurement of diffusive photon density waves by the spread spectrum approach was simulated on a computer[4,5]. The reconstructed temporal profile $V(t)$ is plotted in Figure 1, in comparison with the theoretical prediction. The noise level in the reconstructed temporal profile was around $6.13 \times 10^{-5}$, or 3.2% of the peak value of $V(t)$. It is worthy of notice that less than 41 photons could be detected with TCSPC within the same measurement time.
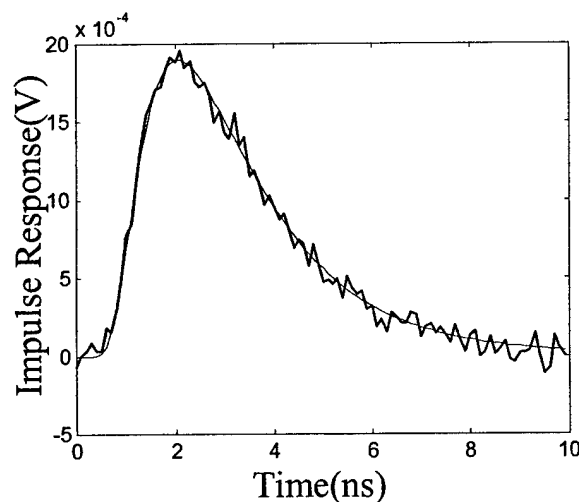


**Figure 1.** Impulse response representing the TPSF of a diffusive photon density wave. Thin curve: theoretical prediction; thick curve: reconstructed from noisy environments.

**KEY RESEARCH ACCOMPLISHMENTS:**
- Built two new diffusive optical imagers for clinical and experimental studies. Our new systems are more compatible, faster, easier to use than the previous PMT-based system;
- Tested and optimized the new optical imagers;
- Assisted clinical studies and collected data from more than 60 patients;
- Did image analysis to interpret the optical images from clinical data;
- Investigated image reconstruction algorithms with finite element method[6,7];
- Investigated image reconstruction with dual mesh method;
- Proposed a novel time-resolved optical imaging system architecture, which is based on spread spectrum excitations and correlation detection.

**REPORTABLE OUTCOMES:**
Journal papers:

[1] Q. Zhu, N. G. Chen, and S. Kurtzman, "Imaging tumor angiogenesis using combined near infrared diffusive light and ultrasound," **Optics Letters**, vol. 28, No. 5, pp 337-339 (2003).

[2] N. G. Chen, and Q. Zhu, "Time-resolved optical measurements with spread spectrum excitations," **Optics Letters**, Vol. 27, No. 20, pp 1806-1808 (2002).

Presentations:
[1] N. G. Chen, H. Xia, D. Piao, and Q. Zhu, "Portable multi-channel multi-wavelength near infrared diffusive light imager," SPIE Photonics West 2003, San Jose, January, 2003.
[2] N. G. Chen, and Q. Zhu, "Spread spectrum time-resolved photon migration imaging system: the principle and simulation results," SPIE Photonics West 2003, San Jose, January, 2003.
[3] Q. Zhu, S. Kurtzman, N. G. Chen, C. Zarfos, M. Huang, and M. Kane, "Breast lesion diagnosis using combined near infrared diffusive light and ultrasound: initial clinical results," SPIE Photonics West 2003, San Jose, January, 2003.
[4] M Huang, T. Xie, N. G. Chen, D. Piao, and Q. Zhu, " 2-D NIR image reconstruction with ultrasound guidance," Proceedings, 2002 IEEE International Symposium on Biomedical Imaging, pp1031-1034 (Washington D.C., 2002).

Funding applied for:
[1] Nan Guang Chen (PI), "Time-resolved photon migration imaging for breast cancer detection – a spread spectrum approach," submitted to DoD, May 2002 (Idea Award, rejected).
[2] Nan Guang Chen (PI), "Novel time-resolved photon migration imaging system for breast cancer detection," submitted to NIH, Jan. 2003 (pending).

## CONCLUSIONS:

I have successfully finished the major part of the Task 2 specified in the statement of work of my proposal. Two new diffusive optical imagers have been built and tested. They have been used in clinical and experimental studies. I also investigated image reconstruction algorithms via different approaches. Clinical data from more than 60 patients has been collected and the initial analysis of acquired images shows strong evidence that ultrasound assisted optical imaging has the excellent potential to become a useful diagnostic tool for breast cancer detection. A novel time-resolved approach has been proposed, which will bring important impact on design of future diffusive optical imagers.

## REFERENCES:

[1] N. G. Chen, H. Xia, D. Piao, and Q. Zhu, "Portable multi-channel multi-wavelength near infrared diffusive light imager," SPIE Proceedings, 4955-25, in press.
[2] Q. Zhu, N. G. Chen, and S. Kurtzman, "Imaging tumor angiogenesis using combined near infrared diffusive light and ultrasound," **Optics Letters**, vol. 28, No. 5, pp 337-339 (2003).

[3] Q. Zhu, S. Kurtzman, N. G. Chen, C. Zarfos, M. Huang, and M. Kane, "Breast lesion diagnosis using combined near infrared diffusive light and ultrasound: initial clinical results," SPIE Proceedings, 4955-10, in press.

[4] N. G. Chen, and Q. Zhu, "Time-resolved optical measurements with spread spectrum excitations," **Optics Letters**, Vol. 27, No. 20, pp 1806-1808 (2002).

[5] N. G. Chen, and Q. Zhu, "Spread spectrum time-resolved photon migration imaging system: the principle and simulation results," SPIE Proceedings, 4955-67, in press.

[6] M. Huang, T. Xie, N. G. Chen, and Q. Zhu, "NIR imaging reconstruction with ultrasound localization," **Applied Optics**, in press.

[7] M Huang, T. Xie, N. G. Chen, D. Piao, and Q. Zhu, " 2-D NIR image reconstruction with ultrasound guidance," Proceedings, 2002 IEEE International Symposium on Biomedical Imaging, pp1031-1034 (Washington D.C., 2002).

**APPENDICES:**
Copies of recent journal papers:
[1] Q. Zhu, N. G. Chen, and S. Kurtzman, "Imaging tumor angiogenesis using combined near infrared diffusive light and ultrasound," **Optics Letters**, vol. 28, No. 5, pp 337-339 (2003).

[2] N. G. Chen, and Q. Zhu, "Time-resolved optical measurements with spread spectrum excitations," **Optics Letters**, Vol. 27, No. 20, pp 1806-1808 (2002).

# Imaging tumor angiogenesis by use of combined near-infrared diffusive light and ultrasound

**Quing Zhu and NanGuang Chen**

*Department of Electrical and Computer Engineering, University of Connecticut, Storrs, Connecticut 06269-2157*

**Scott H. Kurtzman**

*University of Connecticut Health Center, Farmington, Connecticut 06030*

A novel two-step reconstruction scheme using a combined near-infrared and ultrasound technique and its utility in imaging distributions of optical absorption and hemoglobin concentration of breast lesions are demonstrated. In the first-step image reconstruction, the entire tissue volume is segmented based on initial coregistered ultrasound measurements into lesion and background regions. Reconstruction is performed by use of a finer grid for lesion region and a coarse grid for the background tissue. As a result, the total number of voxels with unknown absorption can be maintained on the same order of total measurements, and the matrix with unknown total absorption distribution is appropriately scaled for inversion. In the second step, image reconstruction is refined by optimization of lesion parameters measured from ultrasound images. It is shown that detailed distributions of wavelength-dependent absorption and hemoglobin concentration of breast carcinoma can be obtained with the new reconstruction scheme.   © 2003 Optical Society of America
   *OCIS codes:*   170.0170, 170.3010, 170.5270, 170.7170, 170.3830.

Tumor blood volume and microvascular density are parameters that are anatomically and functionally associated with tumor angiogenesis. During the past decade, modeling of light propagation in the near-infrared (NIR) region, combined with advancements of light source and detectors, has improved diffused light measurements and made possible the application of tomographic techniques for characterizing and imaging tumor angiogenesis.[1,2] However, the NIR technique has not been widely used in clinics, and the fundamental problem of intense light scattering remains. As a result, diffusive light probes a widespread region instead of providing information along a straight line, and tomographic image reconstruction is, in general, underdetermined and ill-posed. Zhu et al.[3] and Chen et al.[4] demonstrated a combined imaging technique, using *a priori* lesion structure information provided by coregistered ultrasound images to assist NIR imaging reconstruction in phantom studies.[3,4] As a result, the NIR image reconstruction is well defined and less sensitive to noise. In this Letter we report on our novel two-step image reconstruction scheme that uses the combined approach and demonstrate its utility in imaging tumor absorption and hemoglobin distributions. It is shown that detailed heterogeneous distributions of wavelength-dependent optical absorption and hemoglobin concentration of a breast carcinoma can be obtained. To the best of our knowledge, such detailed distributions have not been reported in the literature.

A picture of our combined hand-held probe used in clinical studies is shown in Fig. 1(a), and the probe dimensions and optical sensor distributions are shown in Fig. 1(b). The combined probe consists of a commercial ultrasound one-dimensional array located at the center of the probe and optical source and detector fibers distributed at the periphery

and connected to the NIR imager. The NIR imager consists of 12 dual-wavelength source channels and 8 parallel receiving channels.[4] In the transmission part, 12 pairs of dual-wavelength (780- and 830-nm) laser diodes are amplitude modulated at 140 MHz. In the reception part, 8 photomultiplier tubes detect diffusely reflected light from the tissue. Both the amplitude and phase at each source–detector pair are obtained, and the resulting total number of measurements is $12 \times 8 \times 2 = 192$. The combined probe is made of a black plastic plate 10 cm in diameter; therefore, a semi-infinite boundary condition can be used for the NIR measurement geometry. The amplitude and phase measured from the normal side of the breast are used to calculate the background absorption $\bar{\mu}_a$ and reduced scattering coefficient $\bar{\mu}_s'$.[4] In our two-step image reconstruction, we first segment tissue volume into two regions, $L$ and $B$, that contain a lesion as measured from coregistered ultrasound images and background tissue, respectively. We use the Born approximation to
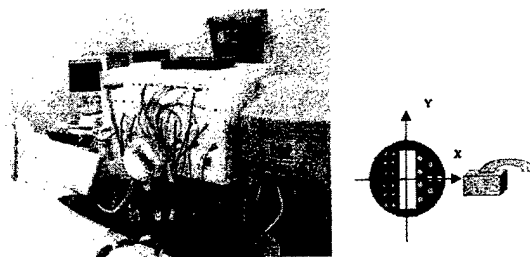


Fig. 1. (a) Hand-held combined probe and a frequency-domain NIR imager. (b) Sensor distribution of the combined probe (diameter, 10 cm). The smaller circles are optical source fibers, and the bigger circles are detector fibers. A commercial ultrasound probe is located at the center and its dimensions are 5.6 cm by 1 cm.

relate the scattered field $U_{sc}'(r_{si}, r_{di}, \omega)$ measured at source–detector pair $i$ to absorption variations $\Delta\mu_a(r')$ in each volume element of two regions within the sample, where $r_{si}$ and $r_{di}$ are the source and detector positions, respectively. We then discretize the lesion volume and the background volume with different voxel sizes (a finer grid for lesion volume and a coarse grid for background). The scattered field can then be approximated as

$$U_{sc}'(r_{si}, r_{di}, \omega) \approx -\frac{1}{D}$$
$$\times \left[ \sum_{Lj} G(r_{vj}, r_{di})U_{inc}(r_{vj}, r_{si}) \int_j \Delta\mu_a(r')d^3r' \right.$$
$$\left. + \sum_{B_k} G(r_{vk}, r_{di})U_{inc}(r_{vk}, r_{si}) \int_k \Delta\mu_a(r')d^3r' \right], \quad (1)$$

where $r_{vj}$ and $r_{vk}$ are the centers of voxels $j$ and $k$ in lesion volume $L$ and background volume $B$, respectively[2], and $U_{inc}(r', r_{si})$ and $G(r', r_{di})$ are the incident wave and the Green function of the semi-infinite geometry, respectively. The matrix form of relation (1) is given as

$$[U_{sd}]_{M\times 1} = [W_L, W_B]_{M\times N}[M_L, M_B]^T, \quad (2)$$

where $W_L = [-\frac{1}{D}G(r_{vj}, r_{di})U_{inc}(r_{vj}, r_{si})]_{M\times N_L}$ and $W_B = [-\frac{1}{D}G(r_{vk}, r_{di})U_{inc}(r_{vk}, r_{si})]_{M\times N_B}$ are weight matrices for the lesion volume and the background volume, respectively; $[M_L] = [\int_{1_L}\Delta\mu_a(r')d^3r, \ldots \int_{N_L}\Delta\mu_a(r')d^3r']$ and $[M_B] = [\int_{1_B}\Delta\mu_a(r')d^3r', \ldots \int_{N_B}\Delta\mu_a(r')d^3r']$ are the total absorption distributions of the lesion volume and the background volume, respectively.

Instead of reconstructing the $\Delta\mu_a$ distribution directly as the standard Born approximation, we reconstruct total absorption distribution $M$ and then divide the total by different voxel sizes of lesion and background tissue to obtain $\Delta\mu_a$ distribution. By choosing a finer grid for the lesion and a coarse grid for the background tissue, we can maintain the total number of voxels with unknown absorption on the same scale of the total measurements. As a result, the inverse problem is less underdetermined and ill-posed. In addition, since the lesion absorption coefficient is higher than that of the background tissue, in general, the total absorption of the lesion over a smaller voxel is on the same scale of total absorption of the background over a bigger voxel, and therefore the matrix $[M_L, M_B]$ is appropriately scaled for inversion. The reconstruction is formulated as a least-squares problem. The unknown distribution $M$ can be iteratively calculated with the conjugate-gradient search method.

The lesion location and volume from coregistered ultrasound is estimated as follows: Since the commercial one-dimensional ultrasound probe that we use acquires two-dimensional ultrasound images in the $y$–$z$ plane ($z$ is the propagation direction) and the two-dimensional NIR probe provides three-dimensional images, the coregistration is limited to an interception plane. However, if we approximate a lesion as an ellipsoid, we are able to estimate its center and radii from two orthogonal ultrasound images and therefore obtain the lesion volume. Three sources of error may

lead to inaccurate estimation of the lesion center and radii and therefore to cause errors in reconstructed optical properties. First, the lesion boundaries may not be well defined in ultrasound images. Second, two separate orthogonal ultrasound images are used to estimate the radii and the center, and these parameters depend on the ultrasound probe position and compression of the hand-held probe. Third, the target volumes or shapes seen by different modalities may be different because of different contrast mechanisms. In the second step, we refine image reconstruction by perturbing the center $c_0$ and then the radii $r_0$ and choosing the optimal set of parameters $(c_{opt}, r_{opt})$.

Clinical studies were performed at the Health Center of the University of Connecticut, and the human subject protocol was approved by the Health Center IRB committee. Patients with palpable and nonpalpable masses that were visible on clinical ultrasound were used as subjects. These subjects were scanned with the combined probe, and ultrasound images and optical measurements were acquired at multiple locations, including the lesion region that was scanned at two orthogonal positions, and a normal region of the contralateral breast scanned at two orthogonal positions.

An example is given in this Letter to demonstrate the use of our reconstruction scheme. Figure 2(a) shows a gray-scale ultrasound image of a palpable lump in a 44-year-old woman. The lesion was located at the 6 to 8 o'clock position of the left breast at approximately 1.5-cm depth. Ultrasound showed an irregular poorly defined hypoechoic mass, and the lesion was considered highly suspicious for malignancy. An ultrasound guided-core needle biopsy was recommended. Biopsy results (after NIR imaging) revealed that the lesion was a high-grade *in situ* ductal carcinoma with necrosis.

Multiple optical measurements at two orthogonal positions were simultaneously made with ultrasound images at the lesion location as well as at approximately the same location of the contralateral normal breast. The fitted average tissue background measured on the normal side of the breast at both wavelengths was $\overline{\mu}_a^{780} = 0.03$ cm$^{-1}$, $\overline{\mu}_a^{830} = 0.05$ cm$^{-1}$, $\overline{\mu}_s'^{780} = 9.22$ cm$^{-1}$, and $\overline{\mu}_s'^{830} = 7.58$ cm$^{-1}$. The perturbations for both wavelengths used to calculate absorption maps were normalized as $U_{sc}'(r_{si}, r_{di}, \omega) = [U_L(r_{si}, r_{di}, \omega) - U_N(r_{si}, r_{di}, \omega)] U_B(r_{si}, r_{di}, \omega)/U_N(r_{si}, r_{di}, \omega)$, where $U_L(r_{si}, r_{di}, \omega)$ and $U_N(r_{si}, r_{di}, \omega)$ were measurements obtained from the lesion region and the contralateral normal region, respectively, and $U_B(r_{si}, r_{di}, \omega)$ was the incident field calculated with fitted background $\overline{\mu}_a$ and $\overline{D} = 1/3\mu_s'$. This procedure cancels unknown system gains associated with different sources and detectors as well as electronic channels. The initial estimates of the lesion center and diameter in two orthogonal ultrasound images were $(0, 0.39$ cm$, 1.7$ cm$)$ and $3.44$ cm $\times$ $4.38$ cm $\times$ $1.76$ cm, respectively. A finer grid of $0.5$ cm $\times$ $0.5$ cm $\times$ $0.5$ cm and a coarse grid of $1.5$ cm $\times$ $1.5$ cm $\times$ $1.0$ cm were chosen for the lesion and background tissue, respectively. The total reconstruction volume was chosen to be $9$ cm $\times$ $9$ cm $\times$ $4$ cm,
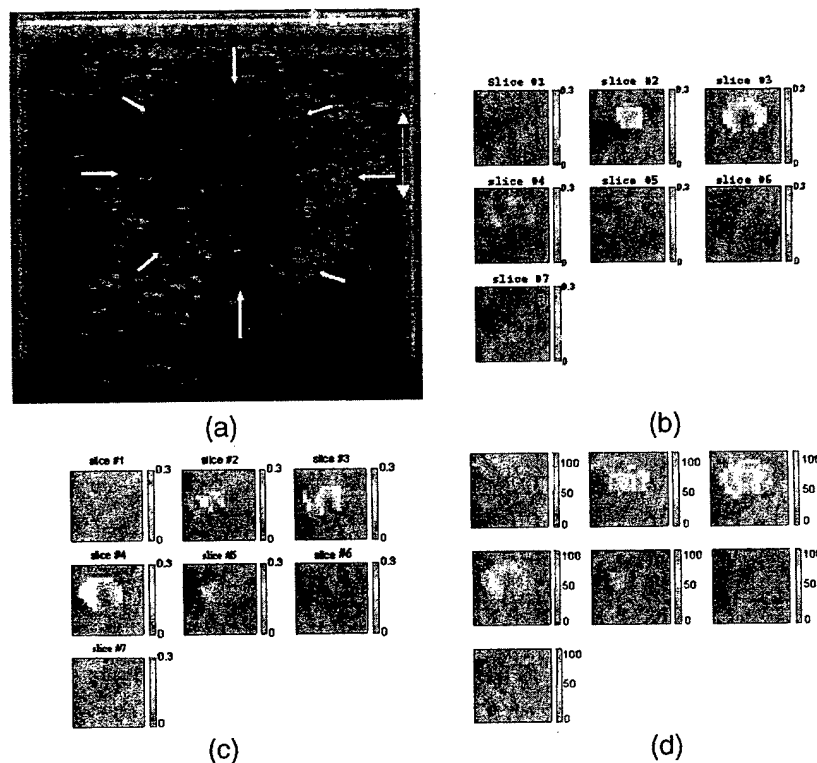
Fig. 2. (a) Gray-scale ultrasound image of a palpable lump of a 44-year-old woman. Ultrasound showed an irregular poorly defined hypoechoic mass, and the lesion was considered as highly suspicious for malignancy. Reconstructed optical absorption maps at (b) 780 nm and (c) 830 nm. The vertical color bars are the absorption coefficient [cm$^{-1}$]. (d) Total hemoglobin concentration map. The vertical color bars are $\mu$mol. The NIR data were simultaneously acquired with the ultrasound image shown in (a). Each image consists of seven slices obtained in 0.5-cm spacing from 0.5 to 3.5 cm in depth. The vertical and horizontal axes correspond to $x$ and $y$ dimensions of 9 cm by 9 cm.

and the total number of voxels with unknown optical absorption was 190, which was of the same order as the 192 total measurements. Image reconstruction was performed with the NIR data simultaneously acquired with the ultrasound image shown in Fig. 2(a). The second-step refined reconstruction revealed optimal lesion centers at approximately (−1.1 cm, 0.3 cm, 1.7 cm) for 780 nm and (−0.9 cm, −0.7 cm, 1.7 cm) for 830 nm and optimal diameters of 4.28 cm × 5.18 cm × 1.96 cm. The detailed absorption maps with high absorption nonuniformly distributed around the lesion boundaries at both wavelengths are shown in Figs. 2(b) and 2(c). By assuming that the major chromophores are oxygenated (oxyHb) and deoxygenated (deoxyHb) hemoglobin molecules in the wavelength range studied, we can estimate the distribution of total hemoglobin concentration as shown in Fig. 2(d). The measured average cancer and background total hemoglobin concentrations were 55.8 $\mu$mol and 20.7 $\mu$mol, respectively.

It is interesting to note that the absorption distributions at both wavelengths as well as the total hemoglobin concentration were distributed heterogeneously at the cancer periphery. To the best of our knowledge, such fine distributions have not been obtained by use of NIR-only reconstruction techniques. However, this finding agrees with the published literature showing that breast cancers have higher blood volumes than nonmalignant tissue because of angiogenesis, especially at the cancer periphery. In addition, the carcinoma reported here had a necrotic core, which could lead to the low absorption observed at both wavelengths in the center region.

## References

1. B. Tromberg, N. Shah, R. Lanning, A. Cerussi, J. Espinoza, T. Pham, L. Svaasand, and J. Butler, Neoplasia **2,** 26 (2000).
2. B. Pogue, S. P. Poplack, T. O. McBride, W. A. Wells, K. S. Osterman, U. Osterberg, and K. D. Paulsen, Radiology **218,** 261 (2001).
3. Q. Zhu, T. Durduran, M. Holboke, V. Ntziachristos, and A. Yodh, Opt. Lett. **24,** 1050 (1999).
4. N. G. Chen, P. Y. Guo, S. K. Yan, D. Q. Piao, and Q. Zhu, Appl. Opt. **40,** 6367 (2001).
5. P. Vaupel, F. Kallinowski, and P. Okunieff, Cancer Res. **49,** 6449 (1989).

# Time-resolved optical measurements with spread spectrum excitation

Nan Guang Chen and Quing Zhu

*Department of Electrical and Computer Engineering, University of Connecticut, Storrs, Connecticut 06269*

We propose a novel method for measuring time-dependent optical quantities. A train of excitation pulses modulated by a pseudorandom bit sequence is used as the light source, and a cross-correlation scheme is used to retrieve the impulse response. Simulation results of the temporal point-spread function of a diffusive wave are provided, as well as experimental results of a fluorescence decay profile. It is demonstrated that our new time-resolved technique can lead to high signal-to-noise ratios and short data acquisition times. A fluorescence-time-dependent suppression process was also been discovered. © 2002 Optical Society of America

*OCIS codes:* 170.3650, 170.6920, 170.5280, 170.6280.

Time-resolved techniques are important in optical instrumentation. Measurements of time-dependent transmittance, reflectance, and fluorescence in response to illumination by an impulse of light always contain rich information that can be used to retrieve the dynamics and other properties of the sample under investigation. Time-resolved photon-migration imaging and time-resolved fluorescence spectroscopy and imaging are good examples of such techniques.

Photon-migration imaging has been emerging as a potential clinical diagnostic modality.[1] Conventional time-resolved photon-migration imaging measures temporal point-spread functions (TPSFs), which can be used for quantitative reconstruction of distributions of scattering and absorption coefficients.[2] Accurate measurement of the rising edge of a TPSF, which is related to that quasi-straightforward propagating component, is desirable for improving spatial resolution.[3,4] Time-resolved fluorescence spectroscopy[5] and imaging[6] have been used in a wide range of research areas such as biosciences, chemistry, and clinical diagnosis. The fluorescence lifetime of a chromophore depends on its characteristic internal structure as well as on its physical and chemical environments. Discrimination of signals related to different fluorescence lifetimes has been exploited to suppress background autofluorescence, improve signal-to-noise ratio, achieve high sensitivity and signal specificity, and measure local environmental parameters such as pH, temperature, and ion concentrations. Fluorescence-lifetime imaging microscopy makes it possible to reveal the biomedical processes and reactions within a cell with high spatial resolution. Determination of fluorescence lifetime is generally made in the time domain, in which short excitation pulses are used.

Currently, the temporal profile of the response to an ultrashort light pulse can be measured with either a streak camera or a time-correlated single-photon counting (TCSPC) system. TCSPC is preferred because its dynamic range and temporal linearity are better than those of streak cameras. A few time-resolved systems for medical optical tomography were reported recently, all of which use the TCSPC technique.[7,8] Nonetheless, the principle of single-photon counting requires that no more than one photon be detected in each cycle. This restriction causes a big problem in data acquisition. The maximal count rate is limited by the repetition rate of laser pulses, the processing speed of electronic devices, and the time span of the impulse response. A typical count rate is 100,000 counts per second, which means that approximately 15–30 are required for acquisition of $10^5$–$10^6$ photons for one temporal profile. In some applications, multiple detection channels are necessary to keep the overall data-acquisition time under control. For example, Schmidt *et al.* reported on a 32-channel time-resolved instrument that needs 10–20 min for a complete scan.[8] It is worthy of mention that far more photon counts are needed for accurate measurement of the intensity of early-arriving photons.

We propose in this Letter a coded excitation and correlation detection mechanism that borrows ideas from spread-spectrum communications. It is well known that a spread spectrum communication system possesses many desirable properties, such as selective addressing capability, low error rate, and interference rejection.[9] A broadband pseudorandom code has only a weak cross correlation with other codes and an autocorrelation function that is analogous to a delta function. Consequently, a receiving system can pick up the correct code sequence, addressing it from environmental noise and interference, and is able to distinguish the same sequence that arrives at different times from multiple paths. This property is utilized in our time-resolved optical system, in which photons detected at different time delays need to be resolved. Better signal-to-noise ratio, shorter data-acquisition time, and low system cost are the expected advantages of our new technique. Our computer simulations have demonstrated the feasibility of a time-resolved photon-migration imaging system based on spread spectrum excitation. We have also built a primitive time-resolved fluorometer and have conducted a series of experiments with it. The exponential decay profile of a long-lifetime dye was successfully retrieved.

The principle of our method is simple and straightforward. We denote by $I(t)$ the time-dependent response of a sample to the excitation of an ultrashort

pulse. A light source continuously modulated with a pseudorandom bit sequence is used to illuminate the sample. So the ac component in the detected signal is proportional to a convolution of the impulse response and the excitation:

$$R(t) = AI(t) * P(t), \qquad (1)$$

where $A$ is the modulation depth and $P(t)$ is an $N$-bit-long pseudorandom bit sequence. $P(t)$ is a maximal length sequence, which has a circular auto-correlation function similar to a delta function:

$$g(\tau) = \langle p(t)p(t - \tau) \rangle$$

$$= \begin{cases} 1 & \tau/T_0 = 0 \\ -1/N & \tau/T_0 = 1, 2, \ldots, N/2; \\ & -1, -2, \ldots, -N/2 \end{cases}$$

$$\qquad (2)$$

in which $\tau$ is the time delay and $T_0$ is the bit period. $g(\tau)$ increases linearly when $\tau$ is within $[-T_0, 0]$ and decreases linearly in $[0, T_0]$. In regions out of $[-T_0, T_0]$, the autocorrelation values are essentially zero when $N$ is big enough. By correlating $R(t)$ with $P(t)$ we have

$$f(\tau) = \langle R(t)P(t - \tau) \rangle = I(\tau) * g(\tau). \qquad (3)$$

Equation (3) is valid when the time span of the TPSF is less than $NT_0$. If $T_0$ is small enough, $f(\tau)$ at a specific delay time $\tau$ is well approximated by $I(\tau)$. When $T_0$ becomes comparable to the time scale of $I(\tau)$, $g(\tau)$ acts as an equivalent temporal gating window. So the impulse response or its integral over a time window can be retrieved by the correlation method.

Time-resolved measurement of diffusive photon density waves by the spread spectrum approach was simulated on a computer. A simulated photon migration imaging system consisted virtually of a four-channel 12.5-Gbit/s pattern generator (MP1775A, Anritsu), a 10-Gbit/s 850-nm vertical-cavity surface-emitting laser transmitter (1780, New Focus), a 12-GHz receiver (1580-A, New Focus), a light-collecting device that effectively increased the detection aperture to 1 mm$^2$, and electronic components such as mixers, filters, and amplifiers. A 4095-bit long pseuodran-dom bit sequence $p(t)$ ($T_0 = 100$ ps) generated by the pattern generator was used to directly modulate the transmitter to generate an optical pulse sequence with a 1-mW peak-to-valley value. The optical fibers of the transmitter and the receiver were embedded in an infinite homogeneous turbid medium and were separated by 5 cm. The reduced scattering coefficient of the medium was 6 cm$^{-1}$, and the absorption coefficient was chosen to be 0.02 cm$^{-1}$. The ideal response of the receiver to a 1-nJ pulse from the transmitter was denoted $V(t)$ and is proportional to the TPSF that can be computed with the diffusion equation. The receiver's response to the pseudorandom normal sequence stimulation was given by

$$M(t) = AV(t) * [P(t) + n_s R_1(t)] + n_d R_2(t), \qquad (4)$$

where $A = 10^{-4}$ and where $R_1(t)$ and $R_2(t)$ were random sequences of normal distribution with a unit standard deviation. Noise levels $n_s = 0.022$ and $n_d = 2$ mV were derived from specifications of the transmitter and the receiver. The correlation can be performed by a mixer (e.g., ZMX-10G from Mini-Circuit) and a low-pass filter. The reconstructed $V(t)$ is compared in Fig. 1 with the original curve. The noise level in the reconstructed temporal profile was $\sim 6.13 \times 10^{-5}$, or 3.2% of the peak value of $V(t)$. Note that fewer than 41 photons could be detected by TCSPC within the same measurement time.

To validate our spread spectrum approach experimentally, we built a time-resolved fluoroscopy system and conducted experiments. The experimental system consists of an ultraviolet LED (NSHU550, Nichia America Corporation) whose output spectrum is centered at 375 nm and a photomultiplier tube (R928, Hamamatsu) that is used to detect fluorescent emissions. A personal computer is responsible for generating the same pseudorandom code as mentioned above, synchronizing input and output, and processing digital signals. A train of pseudorandom voltage signals superimposed upon a dc signal is generated from the analog output port of a multifunction data-acquisition card (PCI-MIO-16E-1, National Instruments) and then is power amplified by a current driver to feed the LED. The update rate for the bit sequence is 10$^5$ bits/s, and the sequence is generated repeatedly. The coded excitation light is directed to a fluorescent sample through a light guide. The fluorescent photons are converted by the photomultiplier tube into electrical signals, which are amplified by a 40-dB amplifier before being digitized by the data-acquisition card. Digital cross correlation is performed on the computer to retrieve the impulse response, i.e., the temporal fluorescence decay profile. A solution of a kind of europium chelate (Quantum Dye, Research Organics) was used as the fluorescence
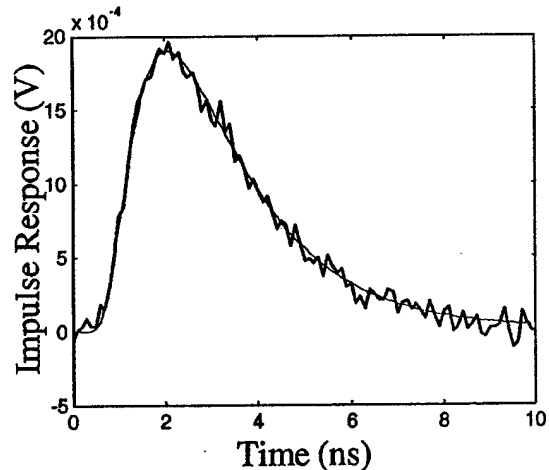


Fig. 1. Impulse response representing the TPSF of a diffusive photon density wave. Thin curve, theoretical prediction; thick curve, reconstruction from noisy environments.
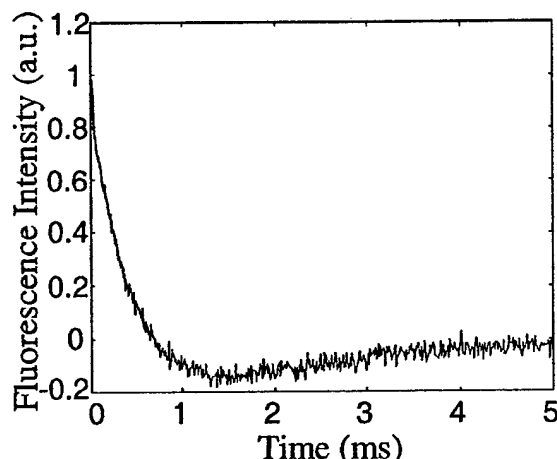
Fig. 2. Florescence decay temporal profile of the solution of eropium chelate, Quantum Dye.

sample. Quantum Dye has a long lifetime (more than 300 $\mu$s), which leads to moderate requirements for system-response speed. The specified excitation wavelength ranges from 360 to 390 nm, and the emission has a peak near 620 nm. An optical long-pass filter was used to separate the emission from the excitation.

An acquired decay profile is plotted in Fig. 2. Initially, the fluorescence intensity decays almost exponentially. However, the intensity crosses zero near ~700 $\mu$s and then remains negative for a few milliseconds. The best fit of profile $I(t)$ with two exponential decay terms is given by

$$I(t) = 1.33 \exp(-t/T_1) - 0.389 \exp(-t/T_2), \quad (5)$$

in which $T_1 = 424$ $\mu$s and $T_2 = 1745$ $\mu$s. The second term on the right-hand side of Eq. (5) represents an interesting phenomenon, which we call time-dependent suppression. To the best of our knowledge, this time-dependent suppression process had not been discovered previously. A simple theoretical explanation of it is as follows: An exciting pulse will bring more molecules to higher energy levels and thus temporarily reduce the population of the ground state. Consequently, the excitation rate is suppressed before the system returns to prepulse status. From the additional time constant $T_2$, one can learn more about radiative and nonradiative transitions involved.

The temporal profile in Fig. 2 was an average over 500 repeated excitations, which took 20.5 s in total. The acquisition time can be reduced to ~4 s if a bit rate of $5 \times 10^5$ bit/s is used. The standard deviation of the intensity is essentially independent of time

and averages 0.022, ~2.3% of the intensity at the origin of time. Suppose that we measure a fluorescence process described by the first term on the right-hand side of Eq. (5) with an ideal TCSPC system and that the photon-counting rate is set to be 200 counts/s. If the probability that a photon is detected in each circle (5 ms) is 1, the relative statistical error at the origin of time can be estimated by

$$\text{err} = \sqrt{\frac{T_1}{C\Delta}}, \quad (6)$$

where $C$ is the total number of photon counts and $\Delta = 10$ $\mu$s is the temporal resolution. For example, we have err = 2.1% when $C = 10^5$. In such a case the total data-acquisition time would be 500 s. Our method can reduce the data-acquisition time by more than tenfold, or significantly improve the signal-to-noise ratio if the same time is spent. Of course, no one will really use single-photon counting for such a slow process. However, the above comparison indicates the great potential of the spread spectrum approach in its future applications in faster optical processes, such as fluorescence decays of nanosecond lifetimes.

To conclude, we have proposed a spread spectrum approach to measuring time-dependent optical processes. Our simulation and experimental results have demonstrated that this new method can remarkably reduce data-acquisition time and (or) improve overall signal-to-noise ratio. In some situations, a much lower system cost can also be expected.

## References

1. A. Yodh and B. Chance, Phys. Today **48**(3), 34 (1995).
2. F. Gao, H. J. Zhao, and Y. Yamada, Appl. Opt. **41**, 778 (2002).
3. N. G. Chen and J. Bai, Phys. Med. Biol. **44**, 1669 (1999).
4. N. G. Chen and Q. Zhu, Proc. SPIE **4250**, 37 (2001).
5. Y. C. Lee, Anal. Biochem. **297**, 123 (2001).
6. C. J. de Grauw and H. C. Gerritsen, Appl. Spectrosc. **55**, 670 (2001).
7. H. Eda, I. Oda, Y. Ito, Y. Wada, Y. Oikawa, Y. Tsunazawa, and M. Takada, Rev. Sci. Instrum. **70**, 3595 (1999).
8. F. E. W. Schmidt, M. E. Fry, E. M. C. Hillman, J. C. Hebden, and D. T. Delpy, Rev. Sci. Instrum. **71**, 256 (2000).
9. R. C. Dixon, *Spread Spectrum Systems* (Wiley, New York, 1976).